Asia Pacific Nanotechnology Forum

2nd Annual Conference

19-21 November 2003
The Hilton Cairns
Tropical Queensland
Australia

in collaboration with the

Australian National Nanotechnology Network

"Oz Nano 03"

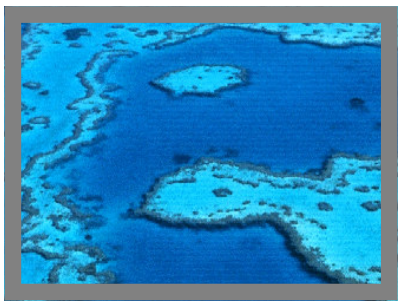

and

International Nanotechnology Showcasing Exhibition

Australian Government
Invest Australia

Australian Government
Department of Education, Science and Training

THOMSON DERWENT

The University Of Queensland

Self-organized silicon quantum dot superlattice prepared by RF magnetron sputtering

E.-C. Cho[1)], Y.-H. Cho[1)], R. Corkish[1)], J. Xia[1)], M. A. Green[1)] and D.-S. Moon[2)]

1) Centre of Excellence for Advanced Silicon Photovoltaics and Photonics, University of New South Wales, Sydney 2052, Australia
e-mail: eccho@unsw.edu.au Fax: (+61 2) 9385 5412

2) School of Electronic engineering, Seoul National University of Technology, Seoul, Korea

1. Introduction

Application of Si nanostrucutures

- Microelectronics with carrier storage
- Optoelectronics with light emission
- Photovoltaics with bandgap opening

Si quantum dots in oxide matrix

- A particle selection formed by electrochemical etching of the silicon substrate (i.e., porous silicon)
- Ion implantation of Si ions into SiO_2 matrix (oxide or quartz)
- Vacuum deposition : Reactive SiO/SiO_2 deposition

Self-organization process of silicon-rich-oxide (SRO, SiO_x, x <2)

$$SiO_x \quad \frac{x}{2}SiO_2 \quad 1 \quad \frac{x}{2} \quad Si$$

- Thermodynamically unstable below 1173oC
- Phase separation of the SiO_x film
- Nano-scale Si quantum dots
  : Annealing temperature
  : Film thickness
  : Stoichiometry of the SiO_x

Quantum dot superlattice in this paper

- alternating SiO_x and SiO_2 layers by co-sputtering of Si and quartz
- Si/SiO_2 superlattie technique

2. Si/SiO_2 superlattice

- Alternating deposition of a-Si and SiO_2 by reactive plasma deposition
- Nanocrystalline Si formation by high temperature annealing
- Continuos Si layer

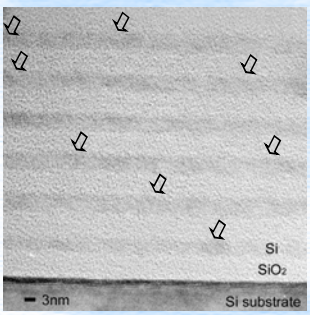

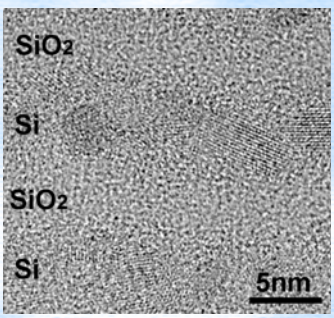

Fig. 1. TEM images of nanocrystalline Si/SiO_2 superlattice with ~4nm thick Si. Si layers in superlattice are continuous (a) and contain the obvious Si nanocrystals (b).

3. Si quantum dot superlattice

SRO deposition instead of the Si layer in Si/SiO_2 superlattice

- SRO – cosputtering of Si and quartz
- SiO_2 – plasma oxide deposition

Diameter of Si quantum dots

- Equal to thickness of SRO

Packing density (Fig.2)

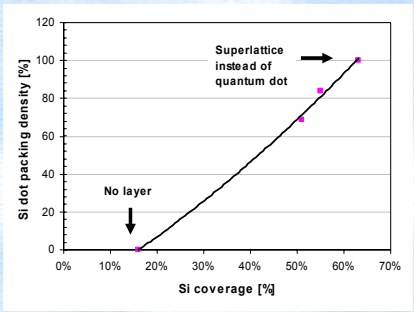

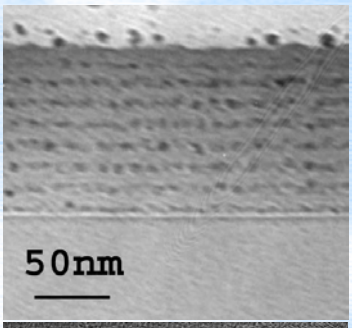

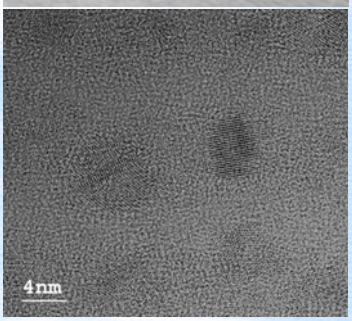

Conclusions

- 50 layers of Si quantum dot in oxide matirx
- Smallest dot size: ~5nm
- Further size reduction with a controlled crystallization process and a reduced SRO thickness

The Special Research Centre for Third Generation Photovoltaics established and supported under the Australian Research Council's Research Centres Scheme

Characterization of Si thickness in single SiO_2/Si/SiO_2 quantum well

E.-C. Cho, R. Corkish, M. A. Green and J. Xia

Centre of Excellence for Advanced Silicon Photovoltaics and Photonics,
University of New South Wales, Sydney 2052, Australia
e-mail: eccho@unsw.edu.au Fax: (+61 2) 9385 5412

1. Introduction

SiO_2/Si/SiO_2 single quantum well by thermal oxidation of SOI wafer

- substrate: SIMOX (Separation by IMplantation of OXygen) or ELTRAN™ (Epitaxial Layer TRANsfer)
- Si thickness to observe quantum confined luminescence
  : < 5nm (Bohr radius of bulk crystalline silicon)

Si thickness characterization in SiO_2/Si/SiO_2 on crystalline Si

- high-resolution transmission electron microscopy (HRTEM)
  : Si thickness by counting a number of Si fringe
  : Long time to prepare the specimens
- Non-destructive optical method
  : Spectroscopic ellipsometry or UV-VIS spectrophotometry
  : in-situ measurement

2. SiO_2/Si/SiO_2 QW characterization

Thermal oxidation of ELTRAN SOI wafers

- Reflectance spectrum by UV/VIS Cary 5 spectrophotometer
- Regression analysis by WVASE32™
- Initial Si thickness calculation from reflectance spectrum (Fig. 1a)
- Multiple oxidation to reduce the superficial Si to ~3nm (Fig. 1b)

(a)

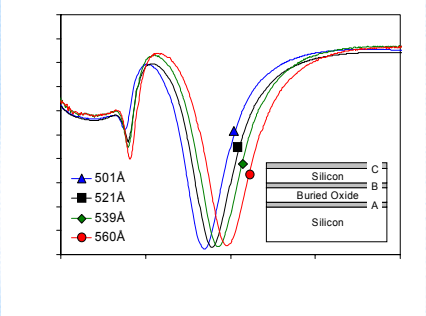

(b)

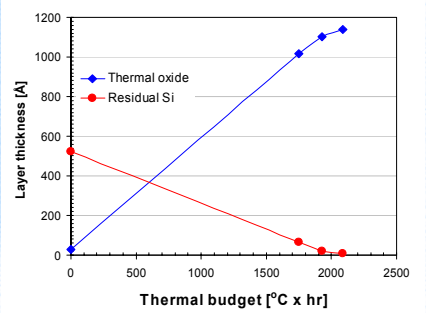

Figure 1. Reflectance spectra of ELTRAN SOI wafer (a) and thicknesses of thermal oxide and residual Si depending on thermal budget (°C × time) (b). Structure model inserted in (a) was used for data regression with the interfaces between BOX/substrate (interface A), c-Si/BOX (interface B), and thermal oxide (native oxide)/c-Si (interface C). The surface SiO_2 layer means either native oxide or thermally grown SiO_2. Interface A and interface B were very thin (~0.2nm) and would not affect the data regression.

Si reflectance spectra near ~3nm thick Si

- wafer for Si QWs – uniform Si thickness chosen by mapping
- No Oxide non-uniformity
- Complete oxidation – Peak valley moves to longer wavelength.
- Ultra-thin Si layer is required to fit reflectance spectrum (Fig. 2)
- E1 transition for 16Å thick Si
- No observation of E1 transition for <1.6Å thick Si

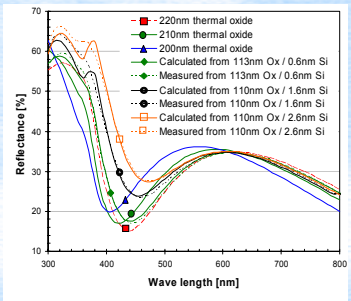

Figure 2. Reflection spectra from thick thermal oxide and SiO_2/Si/SiO_2 QW structures.

3. Comparison with HRTEM

Si thickness by HRTEM is always thicker (5~11 Å) (Fig.3)

(a)

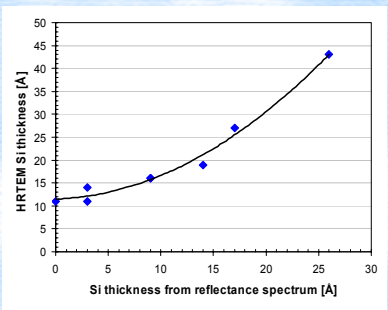

(b)

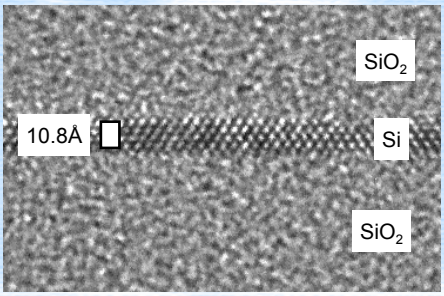

Figure 3. Relation between Si thicknesses from reflectance spectrum and HRTEM (a) and corresponding HRTEM image for the thinnest Si layer (b).

Conclusions

- **Si characterization by UV-VIS reflectance spectrum**
- **Si thickness by HRTEM is always thicker than that from reflectance method.**

The Special Research Centre for Third Generation Photovoltaics established and supported under the Australian Research Council's Research Centres Scheme

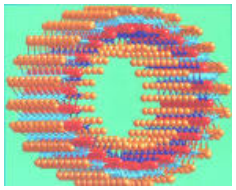

Aluminosilicate Nanotube (IMOGOLITE)

J. Hu, A. McCutcheon, N. Reddy, G.S.K. Kannangara and M.A. Wilson

College of Science, Technology and Environment, LB 1797, Penrith South DC

University of Western Sydney, Australia

University of Western Sydney

Bringing knowledge to life

Naturally Occurring Imogolite

In 1962, the Japanese researchers discovered a crystalline material in volcanic ash soil. This compound had a fixed chemical structure, i.e. $(HO)_3Al_2O_3SiOH$ and a fibre-like appearance under the transmission electron microscope. The new mineral was called *imogolite* (the prefix *imogo* is Japanese for 'glassy volcanic ash') [1].

Properties and Applications

- High surface area: 900 - 1100 m^2/g.
- High anion adsorption capacity for arsenate, cyanide, and phosphate and therefore used in decontamination.
- Low surface acidity, absence of exchangeable cations, regular internal surface and defined porosity.
- Potential space shuttle materials.
- Shape-selective copper-loaded imogolite catalyst [3].

Structure

The imogolite has a tubular structure with an external diamater of ca. 2.5 nm, an internal diameter of 1 nm and lengths varying from several hundreds nanometers to micrometers.

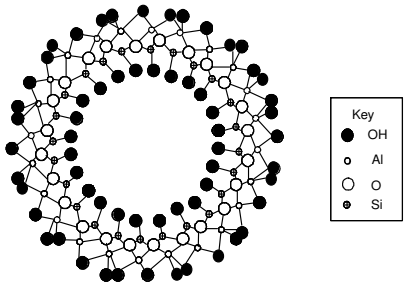

Synthesis & TEM Characterisation

The ^{29}Si labelled imogolite from fused sodium silicate and aluminium perchlorate was synthesised via ^{29}Si labelled SiO_2 and TEM of the product is as follows [4].

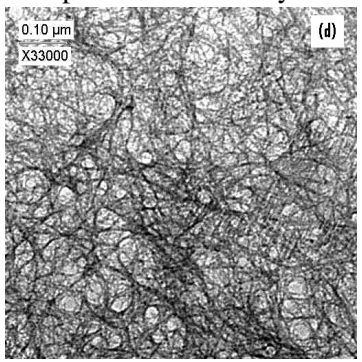

Imogolite and Nanotechnology

- Nanoscale tubular object is considered important building blocks of nanotechnology.
- Oxide nanotubes offer a potentially great diversity of physicochemical properties, accessible by inexpensive and mild aqueous-phase synthesis methods.
- Naturally occurring single-walled aluminosilicate nanotubes (imogolite) are fascinating examples for nanotechnology R&D [2].

IR and NMR Spectroscopic Characterisation

The product imogolite has interesting NMR and infra red spectroscopic properties because of the location of ^{29}Si as isolated silicon tetrahedral but still near neighbours.

In the infra red absorptions are as expected appear at lower wavenumbers due to changes in vibrational bond energies. Linewidths in solid state NMR spectra are dominated by ^{29}Si-^{27}Al interactions so J or dipolar coupling is not observed. Nevertheless by undertaking static and decoupling experiments it was possible to calculate the ^{29}Si-^{29}Si interaction which is about 112.5Hz [5].

[1] Yoshinaga, N., *etal*., *Soil Sci. Plant Nutr.* **1962**, 8, 22. [2] a) Wilson, M.A., *etal*., *Nanotechnology*, **2002**, University of New South Wales Press, Sydney; b) Wilson, M.A., *etal*., *J. Non-Crystalline Solids*, **2001**, 296, 172. [3] a) Imamura, S., *etal., J. Catal*., **1996**, 160, 137; b) Hu, J., *etal*., *J. Catal*., **2000**, 195, 360. [4] Hu, J., *etal*., The Fused Silicate Route to Protoimogolite and Imogolite. *J. Non-Crystalline Solids*, **2003**, submitted. [5] McCutcheon, A., *etal*., ^{29}Si Labelled Imogolite, *J. Phys.Chem. A*. **2003**, in preparation.

Characterisation of the CLIC1 Chloride Ion Channel in Artificial Lipid Membranes, by Scanning Probe Microscopy and Patch-clamp Electrophysiology

Stella M. Valenzuela[1], Mark Berkahn[2], M. Hadi Zareie[2,5], Louise J. Brown[3], Paul M. Curmi[3], Samuel N. Breit[4] and Donald K. Martin[5]

[1]Key University Research Centre in Health Technologies – UTS, [2]Microstructural Analysis Unit – UTS, [3]School of Physics – UNSW, Centre for Immunology – St Vincent's Hospital & UNSW, [5]Institute for Nanoscale Technology – UTS

Summary

CLIC1 (also referred to as NCC27) belongs to a growing family of newly described intracellular chloride ion channel proteins (CLIC). This protein family has the unique feature of being able to move between a soluble (cytoplasm and nucleoplasm) and membrane (plasma and nuclear membrane) bound state. The crystal structure of the soluble form of CLIC1 has recently been elucidated by x-ray crystallography at 1.4 angstrom resolution, but the membrane channel structure remains unknown. Nevertheless, it is most important to understand the structure and behaviour of the CLIC1 chloride channel within its native membrane state.

We have incorporated purified recombinant CLIC1 into artificial lipid membranes. By atomic force microscopy we are attempting to make the first images of CLIC1 in its native membrane state. The combination of AFM imaging and the electrophysiological recordings of ion currents allows us to correlate the function of the channel with visualization of CLIC1 structural transitions including membrane insertion and channel gating. This understanding of the mechanisms for membrane insertion of the protein and its channel gating once in the membrane, allows for the potential use of this protein in a biosensor or artificial cell delivery system.

Results and Methods

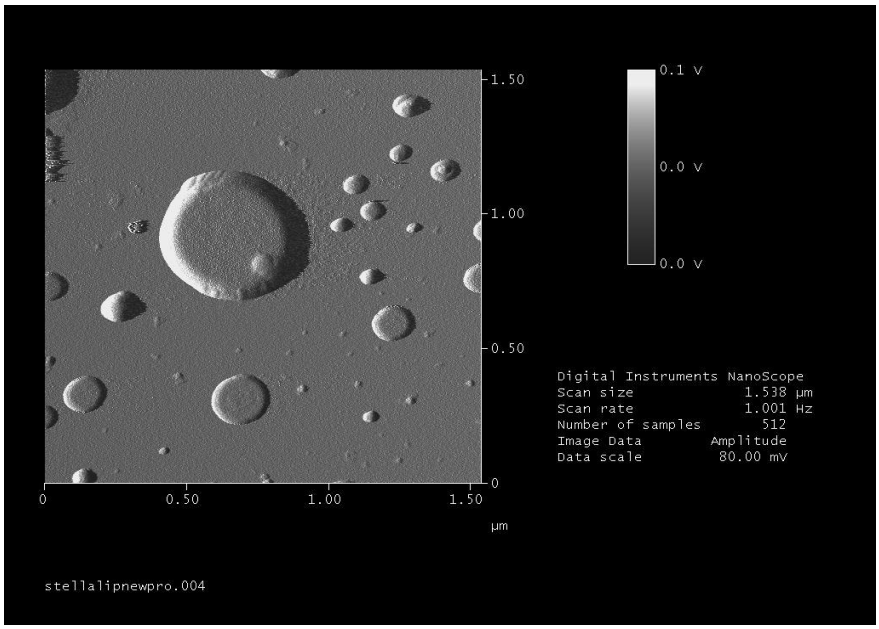

AFM image of liposomes with CLIC1 protein (semi-dry sample) prepared on mica substrate

Artificial liposomes are formed by established methods followed by extrusion through an Avanti Mini Extruder to form vesicles of uniform size ranging from 0.1 to 5.0 microns in diameter.

Electrophysiology

Single-channel patch clamp recording is the major functional assay used for the CLIC1 channel and it is essential in order to correlate structural changes with function. We have established a method at UTS for patch-clamping artificially prepared liposomes with and without incorporated protein.

The Research of the Detonation Nanodiamond Structure by Optical Methods

E.Mironov[1], E.Petrov[2], A.Koretz[3]
1 – CZN, Krasnoyarsk, Russia mir1on1@newmail.ru
2 – FRPC "Altay", Biysk, Russia 659322, post@frpc.secna.ru
3 –State Technical University, Krasnoyarsk, Russia 660074, prcom@kgtu.runnet.ru

One of the principal problems of nano-level science is non-equilibrium. Consequence of this problem is unstable thermodynamic parameters, a confinement for the equilibrium thermodynamics and structural non-homogeneity of condensed matter. The nanodiamond of the detonation synthesis (or the detonation synthesis ultradispersed diamond) [**1,2**] is an object with this non-homogeneity, which is formed by these (non-equilibrium) conditions. 10-20% of detonation nanodiamond mass consists of the functional groups and heteroatoms [**3,4,6**].

This feature is a base for discussion in this work. The density, element analysis, high concentration of functional groups and other parameters are evidence of the fact that the detonation nanodiamond differs considerably from the conventional diamond. That is why there are various interpretations of the UDD, as a diamond-like carbon phase [**4**], a supramolecular system [*G.A.Chiganova, 1999*], a composite-material [*T.M.Gubarevich, and et al 1993*], and all these interpretations were made on the base of considerable experimental results. Certainly, all these experimentalists worked successfully without "special quantum-mechanical properties" of the detonation nanodiamond [**5**].

The structural non-homogeneity is connected with the structural detonation nanodiamond hierarchy (sp^3–hybridized carbon nanograin, explosive cluster 20-60nm). The structurally non-homogeneous primary explosive cluster 20-60nm is a carrier of various functional groups. In addition to reference [**3**], where this idea was introduced, the stability of the primary explosive cluster was observed during the investigation of oxidation [*T.M.Gubarevich, and et al 1993*], study of sedimentation [*G.A.Chiganova, 1999*], and irradiation research [**6,7**]. There are some other indirect data about the stability of the 20-60nm structure. On the whole, by summing up all these reasons, it is possible to say that presence of the nanodiamond impurities is some information on the chemical processes managed by the non-equilibrium. The understanding of these processes is a possible way for the non-equilibrium understanding. Evidently, the equilibrium thermodynamics and the detonation are very different things.

To study the nanodiamond formation, these groups and heteroatom properties and structure were investigated by the methods of infrared (IR) and ultraviolet (UV) spectroscopy.

The nanodiamonds (ultradispersed diamonds – UDD) synthesized from various explosives (trinitrotoluene, hexogen – RDX, trinitrobenzyl, trinitrophenol and so on) were analyzed [**9**]. Nevertheless, in spite of experimental difficulties, the analysis of the structural features of these objects allowed to reconstruct some information about chemical processes from a zone with high non-equilibrium (the reaction zone) [**9**].

On the basis of this hard work, it is possible to characterize the chemical aspect of this reaction zone as a superposition of three basic processes – liberation of conjunction energy, endothermic reactions (the main is molecular nitrogen formation) and competition of some exothermic reactions.

References

[1] Lyamkin AI, Petrov EA, Ershov AP, Sakovich GV, Staver AM, Titov VM (1988) Production of diamonds from explosive substances. Doklady Acad. Nauk SSSR 302 (3): 611-613.
[2] Greiner NR, Phillips DS, Johnson JD, Volk F (1988) Diamonds in detonation soot. Nature 333: 440-442.
[3] Sakovich GV, Gubarevich VD, Badaev FZ, Brylyakov PM, Besedina OA (1990) Aggregation of diamonds obtained from explosives. Doklady Acad. Nauk SSSR 310 (2): 402-404.
[4] Vereschagin AL, Sakovich GV, Komarov VF, Petrov EA (1993) Properties of ultrafine diamond clusters from detonation synthesis. Diamond and Related Materials 3: - 160-162.
[5] Badziag P, Verwoerd WS, Ellis WP, Greiner NR (1990) Nanometer diamonds are more stable than graphite. Nature. 343: 244-245.
[6] Mironov E, Koretz A, Petrov E (2002) Detonation synthesis ultradispersed diamond structural properties investigation by infrared absorption. Proceed. 12th Europ. Conf. "Diamond, Diamond-like materials, carbon nanotubes, nitrides&Silicon carbide", Hungary. Diamond and Related Materials 11 (3-6): 872-876.
[7] Korets AYa, Mironov EV, Petrov EA (2003) IR spectroscopic study of the organic component of ultrafine diamond produced by detonation synthesis. Combustion, Explosion, and Shock Waves (Fizika Gorenia i Vzryva). Translation by Kluwer Academic/ Plenum Publishers. 39 (4): 464-469.
[8] Mironov E, Petrov E, Koretz A (2003) Chemical aspect of ultradispersed diamond formation. Diamond and Related Materials 12 (9): 1472 – 1476.

Controlled complexation of epigallocatechin gallate (EGCg) onto surface-functional nanoporous polymer microspheres : application for a different nanocarrier

Jong-Suk Lee*, *Jin-Woong Kim, Junoh Kim, Ih-Seop Chang

Amore Pacific Corporation R&D Center, 314-1, Bora-ri, Giheung-eup, Yongin-si, Gyeonggi-do, 449-729, Korea

The biological activities of green tea components have been received a great interest, because the polyphenolic fraction of the plant has powerful anti-oxidation properties. Especially, epigallocatechin gallate (EGCg)(fig.1) that is the major component in the polyphenolic fraction has been known to prevent tumorigenesis by protecting cellular components from oxidative damage via free radical scavenging.

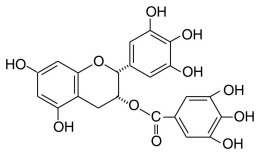

Fig.1 EGCg(epigallocatechin gallate)

However, unfortunately, it is extremely unstable in water-based formulations, which consequently restricts useful applications in pharmaceuticals and cosmetics. In this contribution, we tried to stabilize EGCg with the aid of nanoporous poly(ethylene glycol dimetacrylate-co-acrylonitrile)(poly(EGDMA-co-AN) microspheres. The pore structure of the microspheres was controlled successfully by means of the network phase separation during the polymerization in the suspended monomer droplets. (fig. 2)

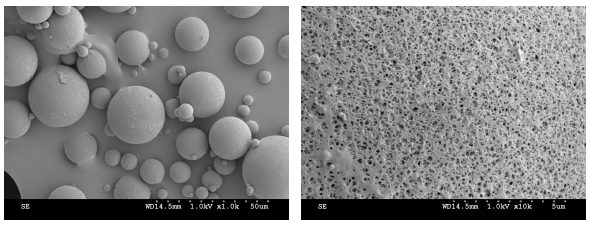

Fig. 2 SEM photographs of nitrile-functionalized poly (EGDMA) microspheres

(Specific surface area: 158.3 m^2/g, Mean pore size: 10.1 nm by BET measurement)

EGCg molecules were incorporated into the porous poly(EGDMA-co-AN) microspheres, which is attributed to the hydrogen bonding between many hydroxyl groups in the EGCg molecules and nitrile groups (CN) on the surface of the microspheres. (scheme 1)

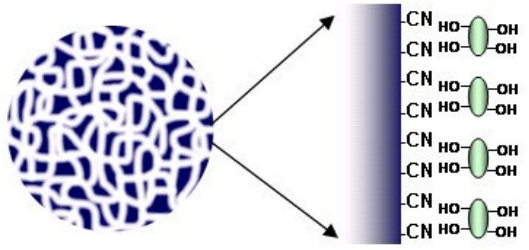

Porous poly(EGDMA-co-AN) Microsphere

complexation of EGCg molecules

Scheme 1. A schematic presentation for the complexation of EGCg molecules onto poly(EGDMA) microspheres

In our study, it was found that the EGCg in the porous poly (EGDMA-co-AN) microspheres showed a distinguished stability, elucidating a high applicability for a different nanocarrier.

Acknowledgment : This work is supported in part from the National Research Laboratory (NRL) program (Project No. 2000-N-NL-01-C-270) by the Ministry of Science and Technology, South Korea

Nanoparticles *via* Delamination of Li/Al Layered Double Hydroxides

Mark I. Ogden,[a] Gordon M. Parkinson[a], Mahua Singh,[a] C.E. Buckley[b] and Joan Connolly[b]

[a] *Nanochemistry Research Institute, Curtin University of Technology, Perth, Australia. E-mail: M.Ogden@curtin.edu.au*
[b] *Materials Research Group, Department of Applied Physics, Curtin University of Technology, Perth, Australia*

Introduction

The preparation of highly dispersed phases from layered materials has attracted considerable interest, with the bulk of studies focussing on dispersions of clay minerals. Layered double hydroxides (LDHs), which have positively charged layers with exchangeable anionic guests, have been less widely studied.[1] The first example of delamination of an LDH was achieved with $Zn_2Al(OH)_6(C_{12}H_{25}SO_4)$ in refluxing butanol.[2,3] More recently $Mg_2Al(OH)_6(C_{12}H_{25}SO_4)$ has been delaminated by heating to reflux in acrylate monomers.[4] Another reported method involved a glycine containing Mg/Al LDH heated to reflux in formamide,[5]

We have been investigating the delamination of the Li/Al LDH, $[LiAl_2(OH)_6]X$, as a possible route to nanoparticulate $Al(OH)_3$.[6] Initial results covering the synthesis and characterisation of these suspensions are described here.

Experimental

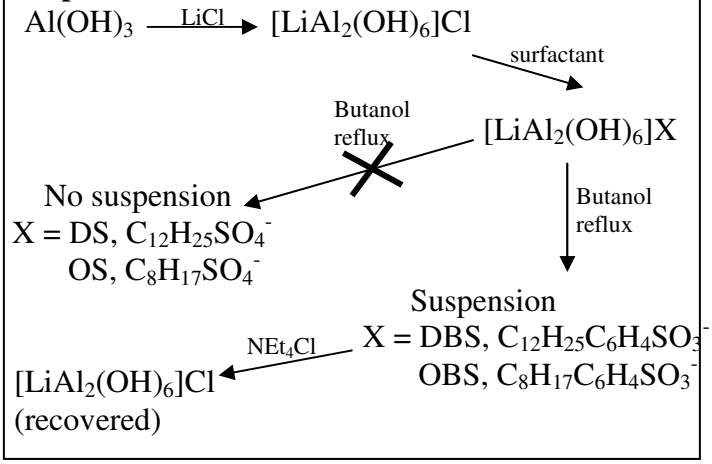

TEM

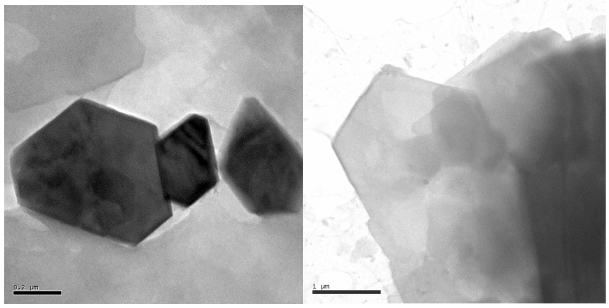

TEM images produced by evaporation of butanol suspensions produced from starting materials of different particle size.

1 A. I. Khan and D. O'Hare, *J Mater Chem*, 2002, **12**, 3191.
2 M. Adachi-Pagano, C. Forano and J. P. Besse, *Chem Commun*, 2000, 91.
3 F. Leroux, M. Adachi-Pagano, M. Intissar, S. Chauviere, C. Forano and J. P. Besse, *J Mater Chem*, 2001, **11**, 105.
4 S. O'Leary, D. O'Hare and G. Seeley, *Chem Commun*, 2002, 1506.
5 T. Hibino and W. Jones, *J Mater Chem*, 2001, **11**, 1321.
6 M. Singh, M. I. Ogden, G. M. Parkinson, C. E. Buckley and J. Connolly, *J Mater Chem*, 2003, submitted.

Powder XRD

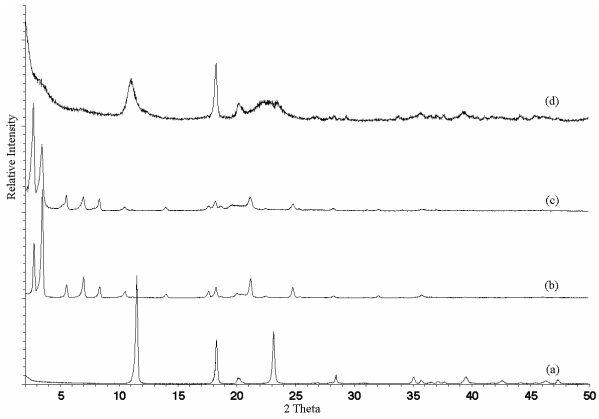

(a) $[LiAl_2\text{-Cl}]$ (b) $[LiAl_2\text{-OBS}]$ (c) $[LiAl_2\text{-OBS}]$(recovered), and (d) $[LiAl_2\text{-Cl}]$(recovered).

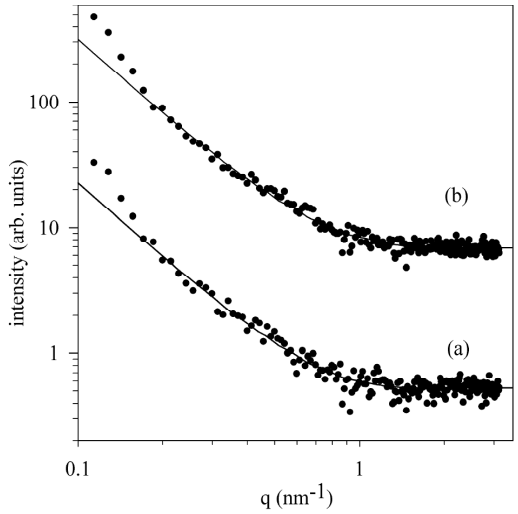

SAXS from $[LiAl_2\text{-DBS}]$ suspension in butanol synthesised from (a) 5 um crystallite size (b) 1um crystallite size gibbsite starting material. The data points in (b) have been scaled by 10 times for clarity. The dots are experimental data points and the line is the fitted model of scattering from cylinders. The error margins on the data points are not shown, but are approximately 10%. The cylinder form was found to fit well to data points for $q > 0.17$ nm^{-1}. The platelet thicknesses were modelled to be 2.8 ± 0.2 and 3.5 ± 0.3 nm for the ~1 μmstarting material and ~5 μm starting material respectively.

Conclusions

- Li/Al LDH delaminated for the first time
- Stability of suspensions dependent on particle size
- First reported example of an LDH delamination process found to depend on the surfactant guest structure

A self-similar array model of single-walled carbon nanotubes

Feng Li[1], Cheng-Hua Sun[1], Hui-Ming Cheng[1], and G.Q.Max Lu[2]

[1]Shenyang National Laboratory for Materials Science, Institute of Metal Research, Chinese Academy of Sciences, P.R.China

[2] The Nanomaterials Centre, School of Engineering, University of Queensland, 4072 Australia

Single-walled carbon nanotubes (SWNTs) promise to be suitable materials in a variety of application areas, such as hydrogen storage. It is well known that SWNTs are apt to form superstructures, such as bundles and ropes. Based on experimental observations, Ebbesen [1] reported the schematic diagram of the fractal-like organization of SWNTs, from the largest bundles down to individual carbon nanotubes. After the fractal superstructures of single-walled carbon nanotubes (SWNTs) was charactered [2], a self-similar array model is induced in this study by self-similar transformation , which was shown in the Fig.1. Before the construction, we assume that SWNTs are infinitely long with a perfect structure and packed with a van der Waals gap G of 0.3147 nm. (12, 12) SWNTs are used and represented as a real circle, while superstructures are represented as imaginary circle, as shown in Fig. 1(c) and (d). For the sake of simplicity, as shown in Fig. 1(c), we also assume that only 7 SWNTs form a bundle with a hexagonal geometry, and all bundles are packed into triangular geometries. In this case, there is one time of self-similar transformation, and the self-similar transformation is marked as t=7 and s=1. Here t is the number of subunits in a unit, and s is the times of self-similar transformation. Pores from several angstroms to over 100 nm can be constructed quantitatively on the basis of the self-similar array model. The pore size distribution (PSD) of SWNTs calculated from the self-similar array model, compared with that obtained from the conventional triangular and square models, shows two additional distribution peaks of pores, inter-bundle pores (marked as γ) and inter-rope pores (marked as δ), respectively. By studying the size effect of SWNT bundles on PSD, it is found that the diameters of γ-pores and δ-pores increase steadily with the increase of the number of SWNTs in a bundle, t. The relative volumes of interstitial pores (marked as β) and γ-pores increase with the increase of t, but the relative volumes of endo-cavities (marked as α) and δ-pores decrease. When the value of t is up to ∽160, however, the relative volumes of all the four kinds of pores are apt to be steady. The originations of pores in SWNTs are discussed by comparing experimental results with calculations of PSD based on the self-similar array model.

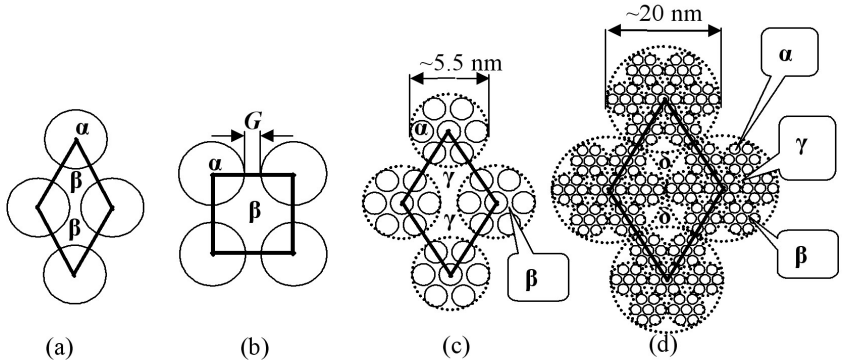

FIG. 1. Cross-sectional view of a (12, 12) nanotube array with a van der Waals gap of 0.3147 nm. Isolated SWNTs are represented as a real circle, while SWNT superstructures are represented as imaginary circle. (a) triangular array; (b) square array; (c) self-similar array with *t*=7 and *s*=1; (d) self-similar array with *t*=7 and *s*=2. Here *t* is the number of subunits in a unit, and *s* is the times of self-similar transformation. The unit cell is shown by using bold lines, diamond for (a), (c) and (d), and square for (b).

Compared with conventional triangular (Fig.1a) and square (Fig.1b) models, the self-similar array model is much closer to real cases of SWNTs because SWNT superstructures are characterized by this model quantitatively, and the characterization range of SWNTs is extended from several nanometers to microns or even larger by adjusting several parameters. Therefore, the theoretical calculations of properties of SWNTs when taking the effect of superstructures into account can be performed on the basis of the self-similar model. To explain the mechanical properties of SWNT ropes, for example, calculations and simulations based on the self-similar array model may be more reliable compared to with those calculations from isolated or triangular model SWNTs. Secondly, pores among SWNT superstructures can be characterized quantitatively, so it is possible to study the effect of those pores on the adsorption properties of SWNTs, especially in the field of hydrogen storage and gas separation, based on the knowledge of pore originations. For hydrogen storage research, for example, the effects of γ-pores and δ-pores in a SWNT sample have never been considered before in those works of theoretical calculations and simulations because those pores cannot be characterized by conventional triangular and square models. Thirdly, from the pore analysis above, we can see that the sizes and relative volumes of the four kinds of pores can be controlled by adjusting the size of SWNT bundles. This is significant in that one can experimentally synthesize SWNT superstructures with particular pore structures. Lastly, we shall notice that β-pores, γ-pores and δ-pores are interconnected with each other and gas molecules can permeate between the three kinds of pores with different diffusion rate. Therefore, the relative volumes of those pores will affect the adsorption dynamics.

Acknowledgements This work was supported by National Science Foundation of China (50025204 and 50032020), and the State Major Basic Research Project of MOST (G2000026403).

References

1 T. W. **Ebbesen**, H. Hiura, J. Fujita, Y. Ochiai, S. Matsui and K. Tanigaki, ***Chemical Physics Letters****, Volume 209, Issues 1-2, 25 June 1993, Pages 83-90,*

2 Cheng-Hua Sun, Feng Li, Zhe Ying, Chang Liu, Hui-Ming Cheng, Submitted

Preparation and Characterization of Polypyrrole-Layered Silicate Nanocomposites

Acharaporn Thuimthad and Rathanawan Magaraphan

The Petroleum and Petrochemical College, Chulalongkorn University, Soi Chula 12, Phyathai Road, Pathumwan, Bangkok 10330, THAILAND

Abstract

Polypyrrole (PPy) was synthesized in the presence of octadecylammonium-montmorillonite (OC-MMT) 1-9 wt% by using ferric chloride as an initiator. The fine black powder was dried and characterized by x-ray diffraction (XRD), thermogravimetry, and FTIR. When using OC-MMT of 9 wt%, the yield is relatively higher than with lower amount of OC-MMT. The results from XRD reveal that the basal spacing of silicate layer retracts to 1.17 nm (for all content of OC-MMT) compared to the spacing in OC-MMT of 2.61 nm. Thermogravemetric results show that PPy has much improved in thermal resistance with higher degradation temperature and lower weight loss of 40 wt% at 650°C while pure PPy has weight loss > 80 wt%. With high loading of OC-MMT, the thermal behavior changes from one transition to two transitions; i.e. first fast degradation followed by much slower degradation for the second transition. By FTIR, it reveals that the amine species still remains in the composites suggesting that the materials prepared are the combination between exfoliated nanocomposite and conventional composite due to partial loss of amine during synthesis. After doping 3 wt% OC-MMT-PPy with DBSA, the XRD pattern shows no peaks below 10 degrees of 2theta suggesting that the doped one is exfoliated nanocomposite. It has better thermal resistance than the undoped one.

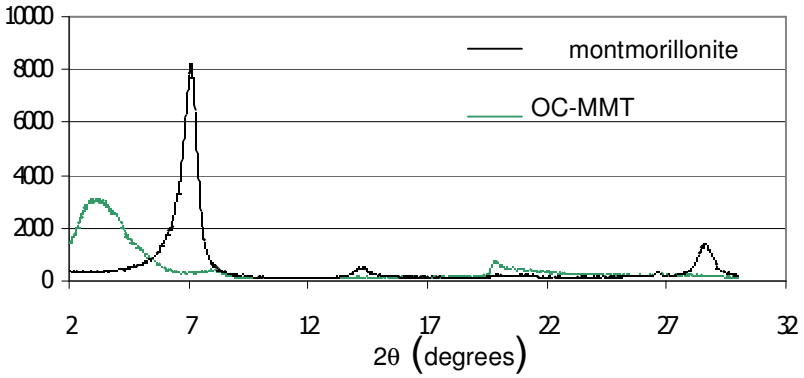

Fig. 1 Diffraction patterns of montmorillonite and OC-MMT
Absorption (arbitary unit)

Table 1 Degradation temperature (Td, °C) and residue content of the nanocomposites

%OC-MMT	Td*	Residue %
0	355.0	48.9
1	382.1	68.7
3	385.0	64.1
6	387.4	62.7
9	387.6	61.1
Doped 3%	366.6	72.2

* as a differential value of the transition (DTG)

Table 2 d-spacing of the silicate layer in the nanocomposites (d-spacing of PPy is from 19.7 Å)

%OC-MMT	d-spacing (Å)	2 theta
OC-MMT	26.91	
1	11.1820	7.9
3, 6	11.2103	7.88
9	11.7774	7.5
Doped 3%	14.6692	6.020
Na-MMT (+ moisture)	12.40 (if no moisture ~ 9.6)	

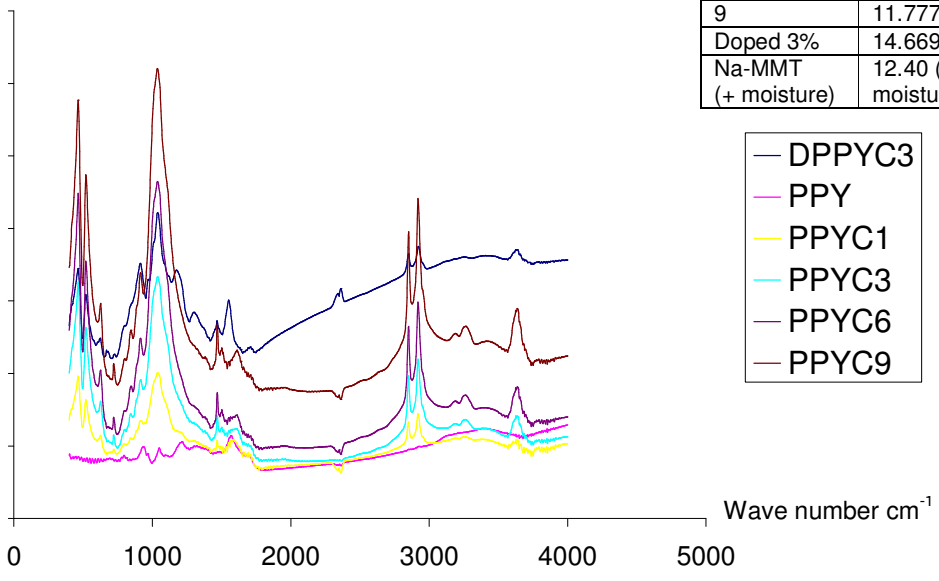

Fig. 2 FTIR of the nanocomposites of PPy (doped and undoped) at several clay content

BN-nanostructures formed by ultra-fast laser ablation

A. V. Rode[1], D. Golberg[2], N. R. Madsen[1], M. Mitome[2], Y. Bando[2], E. G. Gamaly[1], and B. Luther-Davies[1]

[1]*Research School of Physical Sciences and Engineering, Australian National University, Canberra, ACT 0200, Australia*

[2]*Advanced Materials and Nanomaterials Laboratory, National Institute for Materials Science, Tsukuba, Ibaraki 305-0044, Japan*

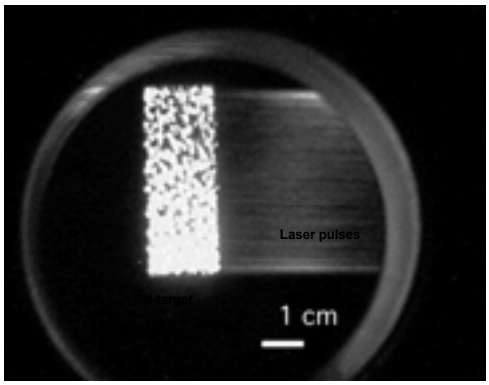

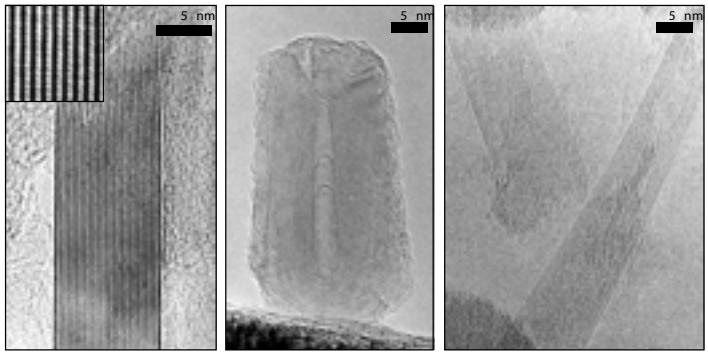

BN-nanorod. Hexagonal type layer stacking is highlighted the inset

A nested nanoparticle

Multi-wall nanotubes

The basis of Ultra-Fast Laser Ablation approach relates to the use of intense and short laser pulses (10^{-13} - 10^{-11} s) delivered to a target with a repetition rate of up to several tens of megahertz.
In such conditions, the ablation process enters the steady-state regime where the continuous influx of atoms from the ablation surface matches the loss due to diffusion and a steady plume is created.

A short laser pulse in combination with optimal pulse intensity for each target material leads to a highest instantaneous ablation rate of up to 10^{30} atoms/(cm^{2}s) during a single pulse. Most importantly, due to the ultra-high-repetition rate the process can produce a dense flow of hot atoms, which is a perfect source for natural formation of unique nanostructures by atom-to-atom attachment.

The ultimate goal of this research is a pioneering application of innovative ultra-high-repetition rate laser ablation of a hexagonal BN target to the formation of a novel BN nanomaterial containing BN nanotubes, in particular, single-walled BN nanotubes.

High-resolution transmission electron microscopy (HRTEM), electron energy loss spectroscopy (EELS), and energy-filtered TEM analysis of the produced nanomaterial revealed a variety of BN nanostructures formed due to the interaction of BN plume with nitrogen ambient. Nanorods, multi-layered nanocages, double-layered "nanohorns", and multi- and single-walled BN nanotubes were discovered in the product. BN nanotubes exhibiting various diameters and numbers of layers, including single-walled nanotubes, were frequently assembled in bundles.

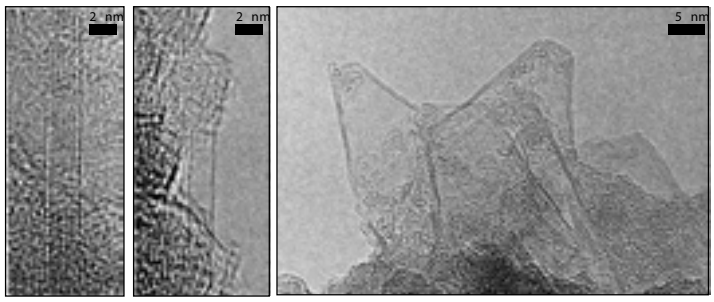

Isolated double-layer nanotube (left) and single-layered nanotube (right).

Two-layered nanohorns. EEL spectrum shows the B and N K-edges at 188 and 401 eV, respectively.
The B/N ratio was calculated to be 0.9 ±0.2.

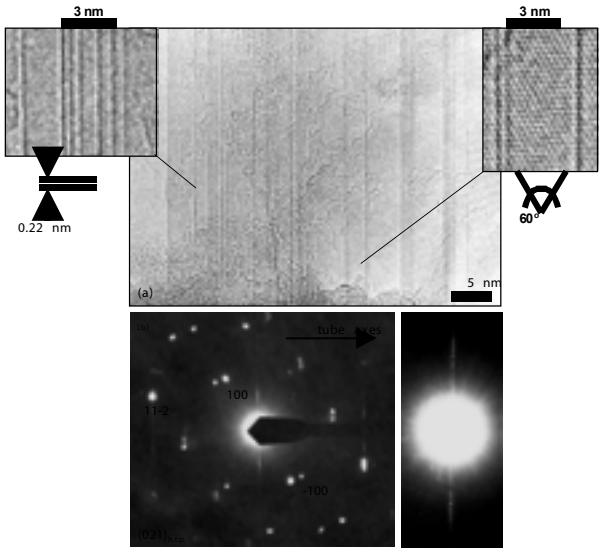

(a) HRTEM image of a BN nanotube assembly residing on the BN flakes; and (b) corresponding diffractionpattern taken from the whole image in (a).

Insets in (a) show two enlarged core regions of the bundle displaying single-layered nanotube fragments with solely zigzag chirality [honeycomb-like dot contrast (60° fringes) or 0.22 nm (10-10) horizontal fringes are seen in the cores];

(c) highlighted central line of the diffraction pattern (equatorial line) exhibiting definite splitting phenomena (superspots) due to packing of nanotubes with various diameters and numbers of layers (but uniform helicity) within the bundle.

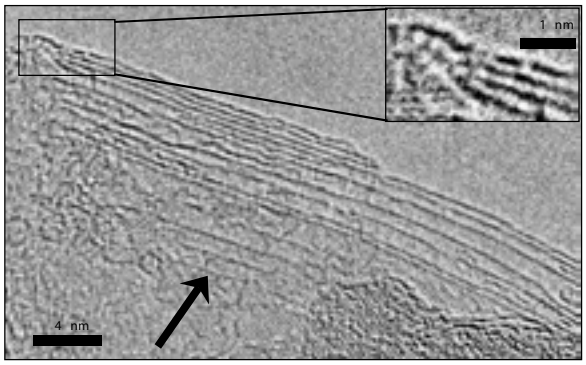

HRTEM image of a tubular bundle containing thin single-layered BN nanotubes, marked with an arrow.

Conclusions

BN nanostructures, i.e. single- and multi-walled nanotubes, "nanohorns", nanoparticles and nanorods, were discovered in a BN material produced *via* ultra-fast laser ablation of a BN crystal by short (60 ps) intense laser pulses with high-repetition-rate (2×10^5 pulses/s) at a nitrogen pressure of ~100 Torr.

The nanostructures display a number of uncommon structural features, not typically seen in BN nanomaterials produced *via* standard synthetic routes, namely:

- disclinations of a graphitic-like sheet characteristic of an odd-number ring defect (pentagon) rather than an even-number ring defect (square); and
- nanotube bundles, constituted of nanotubes with widely varying diameters and numbers of shells, including single-walled nanotubes.

We anticipate that a precise tuning of self-consistent combination of laser-target-filling gas parameters is needed for an efficient production of a specific structure, e.g. single walled BN nanotubes.

Although the presently achieved yield of BN nanostructures was relatively low (~5-10 vol. %) as compared to the primary amorphous-like B-rich phase and bulk hexagonal BN flakes, the structural evidence for unusual nanostructure formation *via* innovative ultra-fast laser vaporization is encouraging and should pave the way to a further detailed search for the optimal parameters of the process (N_2 pressure, catalysts, pulse repetition rate) leading to large-scale production of selective BN nanostructures with unique atomic order.

Hydrogen storage by carbon nanostructures

Ronggang Ding[1,2], G.Q. Max Lu[1], Zifeng Yan[2]

The Nanomaterials Centre, University of Queensland, Brisbane 4072, Queensland, Australia

College of Chemistry and Chemical Engineering, University of Petroleum, Dongying 257061, Shandong, China

Background

Experimental reports of high hydrogen storage capacities in carbon nanostructures are so controversial that it is difficult to assess the application potential. Reliable testing technique needs to be established to estimate the hydrogen storage performance of various forms of carbon nanostructures.

Synthesis and characterization of carbon nanostructures

Catalytic chemical vapor deposition was employed to synthesize the carbon nanostructures. Acetylene was used as carbon source and temperature varied between 500-800 ^{o}C.

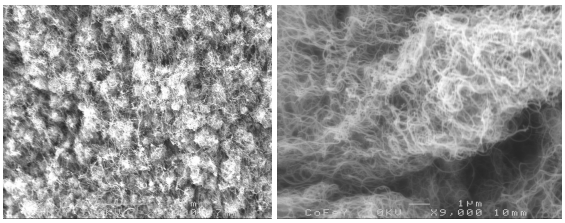

SEM photo of as synthesized carbon nanotubes on Fe/NaY catalyst

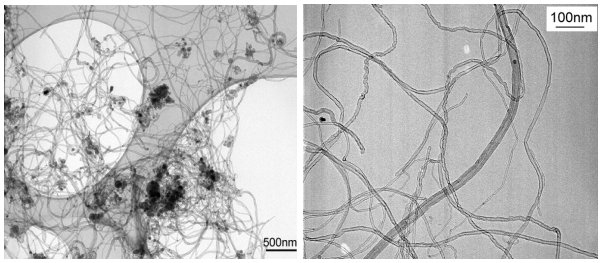

TEM photo of as synthesized carbon nanotubes on Fe/NaY catalyst

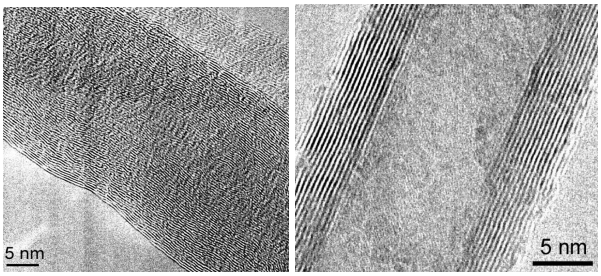

HRTEM photos of as synthesized carbon nanofibers (CNFs) and carbon nanotubes (CNTs) on Fe/γ-Al_2O_3 and Fe/NaY catalyst, respectively

Hydrogen adsorption

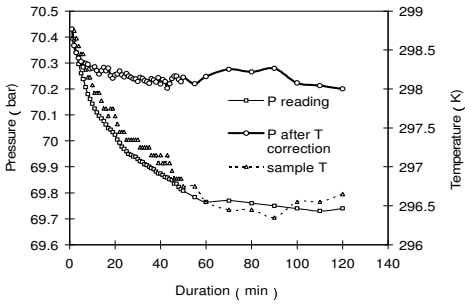

Blank test to estimate the system error

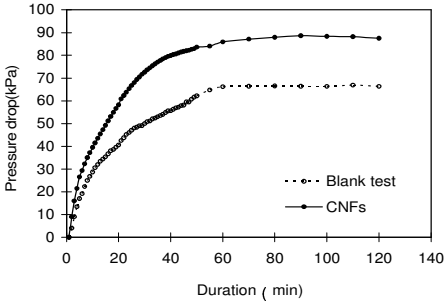

Pressure drop with blank test and CNF samples

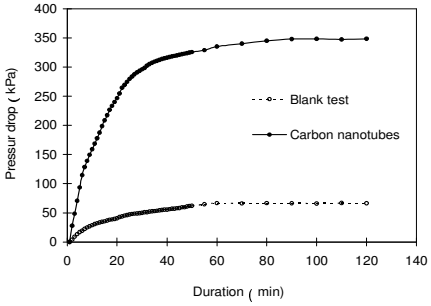

Pressure drop with blank test and CNT samples

Blank test indicated that pressure drop due to the thermal equilibrium return after pressurization of the sample cylinder introduced an error of about 0.9wt% under the specified conditions. The system error is about 0.2wt% after thermal effect correction. The comparison of blank test and actual sample adsorption result gives the reliable adsorption capacities. CNF sample exhibits a poor hydrogen adsorption capacity of 0.27 wt% and CNT a better value of 2.0wt% under 298 K and a pressure of 70 bar.

Microemulsion Templated Nanoporous Silica for Protein Separation Applications

S. Boskovic,[a,b and c] L. Lee,[a] M.L. Gee,[a] A.J. O'Connor,[b] G.W. Stevens[b] and T.W. Turney[c]

a *School of Chemistry and* b *Department of Chemical and Biomolecular Engineering, The University of Melbourne, Victoria 3010, Australia* c *CSIRO Manufacturing and Infrastructure Technology*

INTRODUCTION

In 1992 researchers at the Mobil Research and Development Corporation succeeded in developing a new class of mesoporous molecular sieves: the M41S family.[1, 2] These were the first inorganic materials in the mesopore range with both a narrow pore size distribution and a regular well-defined pore system. The materials were synthesised by combining a silica source with a surfactant in an aqueous environment and a liquid crystal templating mechanism was proposed for their formation.

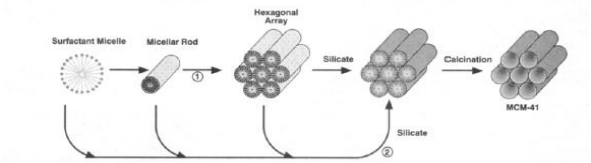

Either the liquid crystal structures present act as templates for the material (path 1) or the addition of the silicate results in a synergistic co-assembly of the micelles into the final liquid crystal type structure (path 2).

Figure 1. Proposed liquid crystal templating mechanism for MCM-41, a member of the M41S family.[2]

In biomolecule separation their promise is twofold; extending the molecular sieving range of zeotype materials into the realm of macromolecules, or as high capacity separation support materials utilising their uniform pore sizes, high surface areas and pore volumes. The pore sizes of the original members of the M41S family probably limits their applications to small biomolecules, however the significant research interest they have generated[3, 4] has led to the development of larger pore materials. One of the most notable of these is the remarkably structured microemulsion templated nanoporous silica foams. These include the Mesocellular Foams (MCF's) first reported by Schmidt-Winkel et al[5] and its structural analogue denoted as MSU-F, reported by Kim et al.[6]

SYNTHESIS

A trimethylbenzene (TMB) in water micoremulsion, stabilised by triblock copolymer acts as a template for the polymerisation of tetraethoxysilane (TEOS) to silica, after which the composite droplets are aged and allowed to pack together. The resulting material is then isolated and calcined, yielding a highly porous 3-D network of spherical voids interconnected via windows.[5]

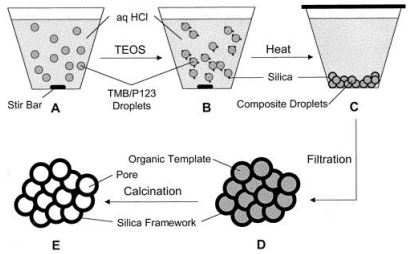

Figure 2. Schematic representation of MCF formation.[7]

STRUCTURE

The size of the spherical voids can be controlled between 22- 42 nm by changing the ratio of TMB/triblock copolymer, which changes the microemulsion droplet size. The size of the window can be controlled by the addition of fluoride; without fluoride windows of around 10 nm occupy up to 30 % of the cells surface forming an array of interconnected spheres, with fluoride windows of up to 22 nm occupy up to 80 % of the cells surface and resemble an array of struts rather than an array of spheres.[5, 7]

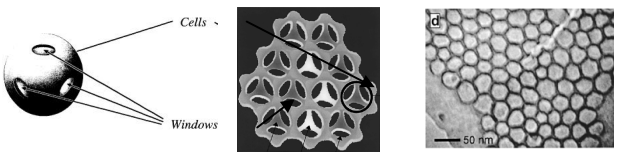

Figure 3. Schematic of the structures of MCF's prepared with fluoride (array of close-packed spheres), without fluoride (array of struts)[5] and a TEM image of MCF prepared without fluoride.[7]

In nitrogen sorption analysis, the pores may be modelled as "ink bottles" using a simplified Broekhoff-de Boer method[8] where the adsorption branch gives the size of the spherical void and the desorption branch gives the window size.

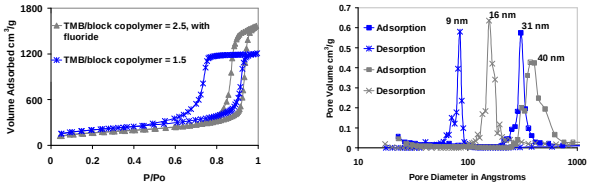

Figure 4. Nitrogen sorption isotherms and corresponding pore size distributions for different MCF samples, synthesised by a modified method of Schmidt-Winkel et al.[7]

AMINO FUNCTIONALISATION

Amino functionality is potentially important as it could be used to target negatively charged biomolecules for separation or it could be used as a surface primer, providing an anchor point for the attachment of other molecules,[9] which may in turn be used for further targeted separations. One such application is Protein A – IgG affinity chromatography, where higher capacity supports have been identified as an industry requirement.[10] Protein A is able to selectively bind to IgG type antibodies and the first step to coupling Protein A to the inorganic support is amino functionalisation.[11]

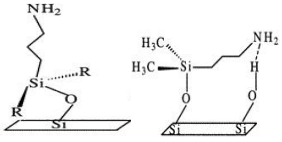

Figure 5. (3-aminopropyl)dimethylsilane orientation, with EDA catalyst and without.[12]

(3-Aminopropyl)dimethylethoxysilane (APDMES) was used to functionalise a mesocellular foam sample synthesised by a modified method of Schmidt-Winkel et al.[7] The functionalisation took place in the vapour phase via a two step method using preadsorbed ethylenediamine (EDA) to catalyse the reaction and lead to amino groups orientated so they are extending from the surface and at double the concentration without EDA.[12]

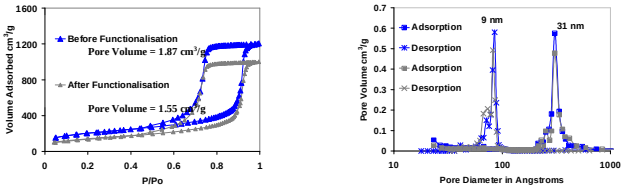

Figure 6. Nitrogen sorption isotherms and corresponding pore size distributions for an MCF sample, before and after amino functionalisation with APDMES and an EDA catalyst.

Nitrogen sorption analysis shows that the isotherm has retained its characteristic shape after functionalisation, which along with the pore size distribution indicates that the materials has maintained its structural integrity. The reduction in pore volume and overall lowering of the isotherm is consistent with the attached groups reducing pore dimensions and increasing the materials weight, which will effect the values as the pore volume is a specific material property, measured on a per weight basis.

REFERENCES

(1) Kresge, C. T. et. al. *Nature* **1992**, *359*, 710.
(2) Beck, J. S. et. al. *Journal of the American Chemical Society* **1992**, *114*, 10834.
(3) Polarz, S. et. al. *Journal of Nanoscience and Nanotechnology* **2002**, *2*, 581.
(4) Davidson, A. *Current Opinion in Colloid and Interface Science* **2002**, *7*, 92.
(5) Schmidt-Winkel, P. et. al. *Journal of the American Chemical Society* **1999**, *121*, 254.
(6) Kim, S. S. et. al. *Chemical Communications* **2000**, 1661.
(7) Schmidt-Winkel, P. et. al. *Chemistry of Materials* **2000**, *12*, 686.
(8) Lukens, W. W. J. et. al. *Langmuir* **1999**, *15*, 5403.
(9) White, L. D. et. al. *Journal of Colloid and Interface Science* **2000**, *232*, 400.
(10) McCue, J. T. et. al. *Journal of Chromatography A* **2003**, *989*, 139.
(11) Weetal, H. H. et. al. *Applied Biochemistry and Biotechnology* **1989**, *22*, 311.
(12) Kanan, S. A. et. al. *Langmuir* **2002**, *18*, 6623.

Near field optics of metallic nanoparticle arrays

T. J. Davis[1*], S. Mayo[1], G. Rosolen[2], A. Roberts[3]

[1] *CSIRO MIT, Private Bag 33, Clayton South, VIC 3169*
[2] *CSIRO ICT Centre, PO Box 76, Epping , NSW 2121*
[3] *School of Physics, The University of Melbourne, VIC 3010*

**Phone: +61-3-9545 2881, email: tj.davis@csiro.au*

With the continuing trend to reduce the size of opto-electronic devices, an understanding of the interaction of light with nano-scale structures is becoming increasingly important [1, 2]. These structures lie in a size range below the wavelength of light so that near-field or evanescent optical fields dominate. Collective interactions between nano-scale components can have a strong influence on the optical far field, opening up new possibilities for the manipulation of the light. For example, the interaction of the electromagnetic fields with metals can produce oscillations of the electron plasma at the surface of the metal (surface plasmons) [3]. For configurations of metal nano-structures, this resonance can enhance the electromagnetic field by many orders of magnitude depending on the specific morphology of the structures and their proximity to one another [3, 4]. Control of these fields and the inter-conversion between them and the radiating fields is important for creating novel optical materials and devices. Possibilities include the creation of materials with negative refractive index [5], or materials based on asymmetric nano-particles with enhanced nonlinear optical properties such as second harmonic generation [6]. We have begun a systematic study of the effects of material type, shape and proximity on the optical near-field interactions using electron beam lithography to control the placement and geometry of nano-structures. Metal films are deposited on a transparent substrate and patterned using the CSIRO electron beam lithography (EBL) facilities in Melbourne and in Sydney. This poster describes the work in progress and our results to date.

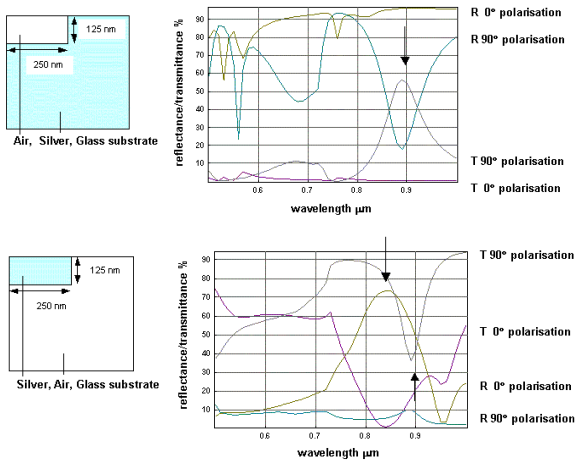

Figure 1. The calculated optical spectra associated with an array of holes in a silver film and an array of silver particles. The arrows indicate plasma oscillation effects.

An electric field applied to an air-filled channel between two metal surfaces induces an electromagnetic disturbance with a dispersion curve related to the dielectric constants of the metal and the width of the channel [7]. The dispersion exhibits two modes - a low and a high frequency mode. For a thin film perforated with an array of sub-wavelength holes the high frequency mode can be excited by light incident at the top surface that can result in anomalous transmission or reflection [8]. Using the technique of Rigorous Coupled Wave Analysis [9, 10] we have modelled the interaction of light with a periodic array of sub-wavelength structures. Figure 1 shows the optical spectra of a 100 nm thick silver film on a glass substrate patterned with an array of rectangular holes and 100 nm thick silver particles (period 500 nm). The model predicts strong transmissions in the near infrared that are related to the existence of plasmon modes, as observed by Ebbesen et al. [8].

To investigate these effects experimentally we are developing processes using electron beam lithography to create two-dimensional arrays of nano-structures from a variety of materials with a range of geometries and spacing. CSIRO has two e-beam systems that can be used for this purpose. One is a commercial instrument, the Leica EBMF 10.5 that has a resolution of about 100 nm but with the capability of writing over areas as large as 100 mm square. The other is a modified SEM system with a resolution below 50 nm but with a restricted writing area. To develop the process, test samples were prepared using a 100 nm thick chromium film on a quartz substrate. The plate was spin-coated with 100 nm thick PMMA resist and exposed with a dose of 250 µC/cm^2. The structure was 9 mm square, the target hole size was 240 nm diameter and the array period was 500 nm. Analysis after development shows a variation in the dimension of the resist where it contacts the chromium, indicating a variation in the dose. The cause of this was traced to instability in the electron beam current associated with an ageing electron source filament. To evaluate the etching procedures, the chromium film was etched in a solution of $2NH_4NO_3.Ce(NO_3)_3.H_2O$, HNO_3 and water heated to 30 Celsius. Following removal of the resist, AFM scans of the resulting film verified the presence of sub-wavelength holes (figure 2). The variation in the diameter may be related to the problems with the e-beam exposure. Once the process parameters are under control a variety of nano-scale patterns will be created using silver, which has a high dielectric constant in the optical region. We aim to verify the prediction of the model using spectroscopy and Near Field Scanning Optical Microscopy to design nano-structures that are resonant in the visible spectrum.

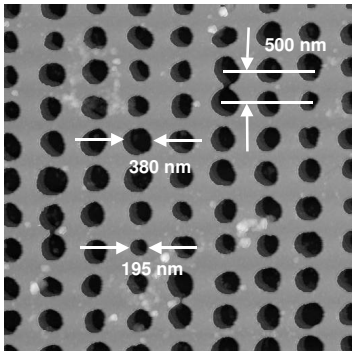

Figure 2. AFM scan of holes in a chromium film created using e-beam lithography.

References

[1] M. Ohtsu, K. Kobayashi, T. Kawazoe, S. Sangu, T. Yatsui: IEEE J. Selected Topics Quantum Electronics **8**, 839 (2002)
[2] Y. Shen, C.S. Friend, Y. Jiang, D. Jakubczyk, J. Swiatkiewicz, P.N. Prasad: J. Phys. Chem. B **104**, 7577 (2000)
[3] A. V. Zayats, I. I. Smolyaninov: J.Opt. A: Pure Appl. Opt. **5**, S16 (2003)
[4] V. M. Shalaev, R. Botet, J. Mercer, E. B. Stechel: Phys. Rev. **B54**, 8235 (1996)
[5] C. Luo, S. G. Johnson, J. D. Joannopoulos: Appl. Phys. Lett. **81** (13) 2352 (2002)
[6] H. Tuovinen *et al.*, J. Nonlinear Optical Physics **11** (4) 421 (2002)
[7] H. Raether: *in Physics of of thin films*, ed. G. Hadd, M. H. Francombe, R. W. Hoffman, **9** 145 (1977)
[8] T. W. Ebbesen, H. J. Lezec, H. F. Ghaemi, T. Thio, P. A. Wolff: Nature **391** 667 (1998)
[9] M. G. Moharam, E. B. Grann, D. A. Pommet, T. K. Gaylord: J. Opt. Soc. Am. A **12** 1068 (1995)
[10] M. G. Moharam, D. A. Pommet, E. B. Grann, T. K. Gaylord: J. Opt. Soc. Am. A **12** 1077 (1995)

The authors wish to thank Russell Marnock for operating the e-beam system and Brett Sexton for assistance with the AFM.

[illegible]

[illegible]

[illegible]

[illegible]

[illegible]

[illegible]

[illegible]

Aim

Using “DNA glue” to locate components, and to self[illegible]

[illegible]

How will this be achieved?

[illegible]

Why DNA?

[illegible]

DNA Self-assembly

[illegible]

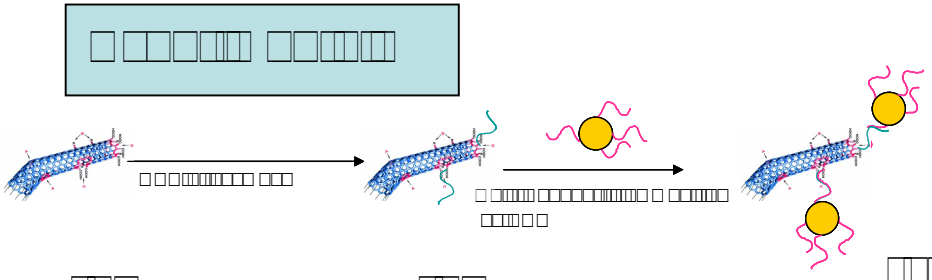

[illegible]

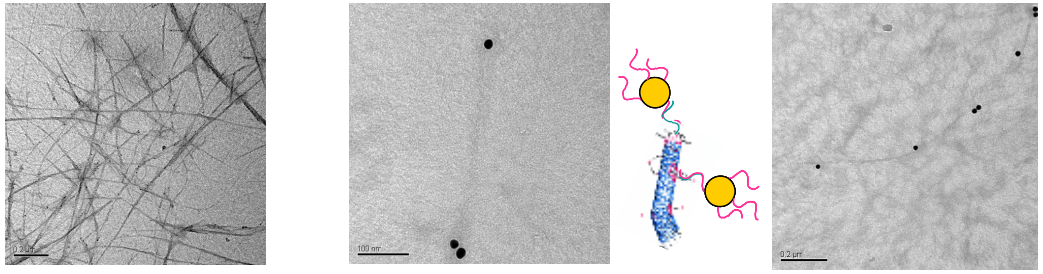

[illegible]

[illegible]

[illegible]

University of Western Sydney
Bringing knowledge to life

Bachelor of Science (Nanotechnology)

Need For This Degree at UWS

Significant scientific and technological developments have led to increased demand for graduates with skills in the rapidly expanding field of nanotechnology. This field draws on the strengths of all the sciences including chemistry, physics, biology and engineering. Providing education and training from a multidisciplinary perspective to a new generation of graduates is absolutely essential.
To satisfy needs and demands, UWS is offering a new specialist undergraduate degree course in the cutting edge science of nanotechnology. The program aims to attract high-achieving students, resulting in high-calibre graduates who will secure employment in the industries of Greater Western Sydney and beyond.

Brief Description of the Course

The three year program will be offered at the Campbelltown campus, although some units will be available at Penrith. It is a comprehensive course that has been designed to provide a strong foundation in the basic sciences and to integrate these sciences in the field of nanotechnology. The comprehensive nature of the course will enable graduates to understand and appreciate the scope of nanotechnological applications.

Resources Available

UWS is equipped with Scanning Electron Microscopy, Atomic Force Microscopy, X-ray diffraction and Nuclear Magnetic Resonance Spectroscopy facilities. The NMR facilities include capabilities to carry out solid state and solution state experiments, and imaging capabilities.

Links with Industries

UWS has joined forces with the Federal Government to bring nanotechnology to business and industry in the Campbelltown-Camden region, helping them to identify ways to incorporate nanotechnology into manufacturing. Students will visit industry and research institutions to see state of the art technology and will recognise wide-ranging applications that have the potential to revolutionise a number of industries. It creates opportunities for industry-based projects for students and great encouragement to UWS academics to establish links through UWS-Partnership funding programs. UWS has already been successful in receiving ARC linkage funds with an industry partner, Kirk Engineering Group.

For further information FREECALL 1800 897 669,
or visit www.uws.edu.au/studyoptions

Ball Milling Assisted Growth of Aligned Carbon Nanotubes

Ying Chen[1] and Lewis T. Chadderton[2]

[1]*Department of Electronic Materials Engineering, Research School of Physical The Australian National University,* *Ying.chen@anu.edu.au*

[2]*Atomic and Molecular Physics Laboratories Sciences and Engineering Canberra, ACT 0200, Australia* *www.rsphysse.anu.edu.au/nanotube/*

Ball Milling vs. Nanotubes

The modern technique of high-energy ball milling has a large range of applications in the processing of nanotube materials, including:

- synthesis of C and BN nanotubes,
- opening of closed nanotubes,
- cutting of long nanotubes into short lengths,
- assisting functionization.

We show here that ball milling can also assist in the

Without Ball Milling Treatment

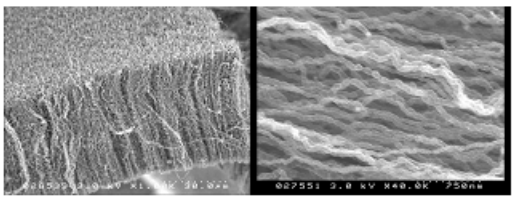

1000 °C / 5 minutes, Ar-5%H_2 flow of 50 cm^3/min

With Ball Milling Treatment

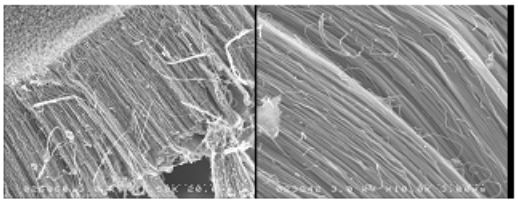

PcFe milled for 100 hr before heat treatment at 1000 °C for 5 minutes in Ar-5%H_2 flow of 50 cm^3/min.

Summary

a prior ball milling treatment of iron phthalocyanine improves the quality of aligned nanotubes. Long, straight and parallel nanotubes have been obtained. The diameter of the aligned nanotubes can be controlled under specific conditions. This improved control of the growth of aligned nanotubes is due to the increased reactivity of phthalocyanine after the ball milling treatment.

Ball Milling Devices

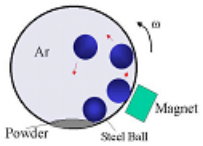

Carbon Nanotubes Growth

- Precursor: iron phthalocyanine (PcFe)
- Pyrolysis conditions:
  - 1000 °C / 5 minutes
  - Ar-5%H_2 gas (50 cm^3/min)

Mechanically Activated Structures

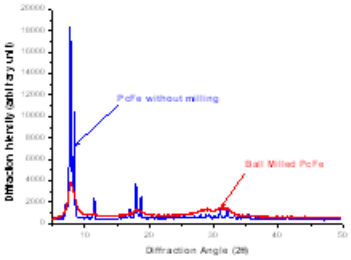

Ball milling produces nanosized and disordered structure.

Thermogravimetric Analysis

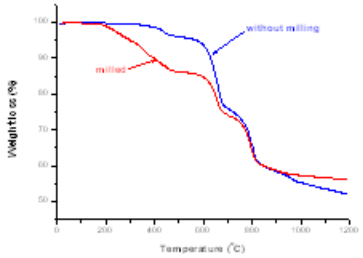

Ball milling reduces vaporization temperature.

Controlled Growth of Boron Nitride Nanotubes in the Mechano-Thermal Process

Y. Chen[1], J. Fitzgerald[1], J.S. Williams[1] and J. Zou[2]

[1] Research School of Physical Sciences and Engineering, The Australian National University, Canberra, ACT 0200, Australian;
[2]Electron Microscopy Unit, University of Sydney, Sydney, Australia

Mechano-thermal method

Two-step process:

1. mechanical milling
2. thermal annealing

Advantages:

- C and BN nanotubes
- Large quantity production (~Kg)
  using lab oratory-scaled equipment
- Controlled nanostructure and size
- Low production costs
- Improved understanding of formation mechanisms

NT02 6

Excellent properties of BN nanotubes

1. Similar superb mechanical properties
2. Better resistance to oxidation
3. Better thermal conductivity
4. Stable electronic properties

Higher resistance to oxidation

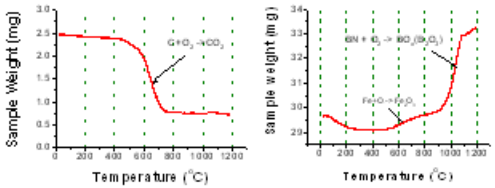

Thermogravimetric analysis of C and BN nanotubes heating (20 °C /min) in air flow (10 ml/min)

NT02 4

Large-sized milling devices

Milling capability up to Kg

NT02 9

High Yield (up to 85%)

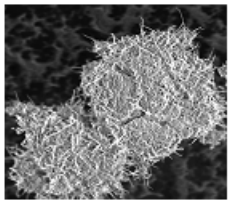

B milled for 150hr and annealed at 1200 °C/8hr

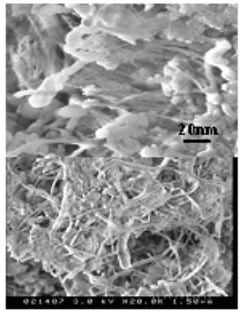

NT02

Iron particle catalyzed growth

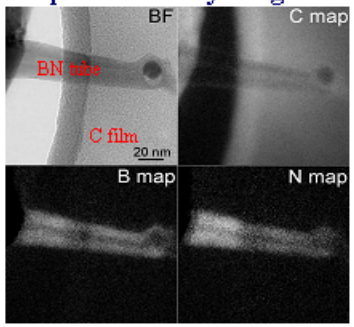

EELS analysis

NT02 29

Boron milled in a ceramic mill (tungsten carbide) annealed at 1200 °C

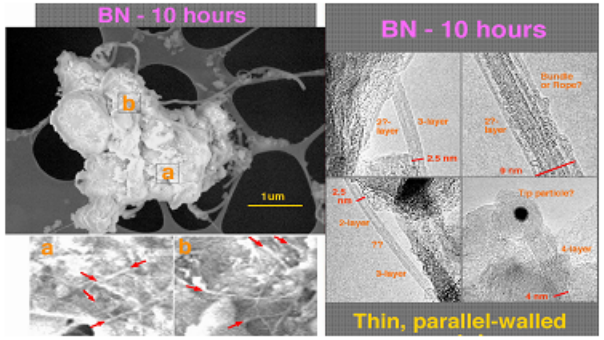

Boron milled in a ceramic mill (tungsten carbide) annealed at 1200 °C

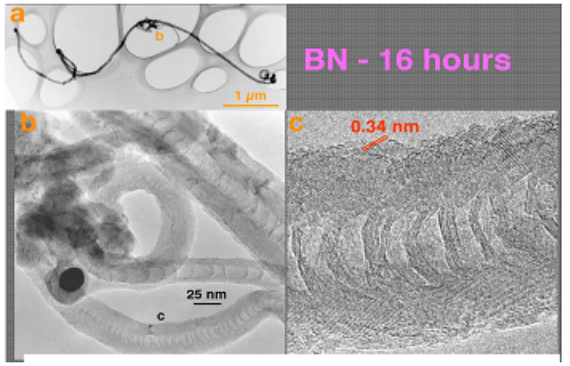

NT02 19

Summary

Mechano-thermal Process

1. Large quantity of high yield BN nanotubes
2. Controlled structure and size
3. Better understanding of formation process

Step 1: ball milling → nucleation

Step 2: thermal annealing → growth